(12)

AD

AD-E401 480

AD-A167 784

TECHNICAL REPORT ARAED-TR-85017

# A SAMARA-TYPE DECELERATOR

WALTER KOENIG
ROY KLINE



MARCH 1986

US ARMY ARMAMENT MUNITIONS & CHEMICAL COMMAND
ARMAMENT R&D CENTER

U. S. ARMY ARMAMENT RESEARCH AND DEVELOPMENT CENTER
ARMAMENT ENGINEERING DIRECTORATE
DOVER, NEW JERSEY

The views, opinions, and/or findings contained in this report are those of the author(s) and should not be construed as an official Department of the Army position, policy, or decision, unless so designated by other documentation.

The citation in this report of the names of commercial firms or commercially available products or services does not constitute official endorsement by or approval of the U.S. Government.

Destroy this report when no longer needed. Do not return to the originator.

ERRATA

AD-E401 480

TECHNICAL REPORT ARAED-TR-85017

# A SAMARA-TYPE DECELERATOR

WALTER KOENIG
ROY KLINE

MARCH 1986

Page 3, lines 13 and 14 are changed to read:

At steady state, $\dot{\omega}_{zp} = 0$; therefore

$$M_z = (I_{yp} - I_{xp})\ \omega_{xp}\ \omega_{yp}$$

April 1986

UNCLASSIFIED

SECURITY CLASSIFICATION OF THIS PAGE (When Data Entered)

| REPORT DOCUMENTATION PAGE | | READ INSTRUCTIONS BEFORE COMPLETING FORM |
|---|---|---|
| 1. REPORT NUMBER<br>Technical Report ARAED-TR-85017 | 2. GOVT ACCESSION NO.<br>AD-A167784 | 3. RECIPIENT'S CATALOG NUMBER |
| 4. TITLE (and Subtitle)<br>A SAMARA-TYPE DECELERATOR | | 5. TYPE OF REPORT & PERIOD COVERED<br>Final<br>6. PERFORMING ORG. REPORT NUMBER |
| 7. AUTHOR(s)<br>Walter Koenig<br>Roy Kline | | 8. CONTRACT OR GRANT NUMBER(s) |
| 9. PERFORMING ORGANIZATION NAME AND ADDRESS<br>ARDC, AED<br>Armament Technology Div (SMCAR-AET-A)<br>Dover, NJ 07801-5001 | | 10. PROGRAM ELEMENT, PROJECT, TASK AREA & WORK UNIT NUMBERS |
| 11. CONTROLLING OFFICE NAME AND ADDRESS<br>ARDC, IMD<br>STINFO Div (SMCAR-MSI)<br>Dover, NJ 07801-5001 | | 12. REPORT DATE<br>March 1986<br>13. NUMBER OF PAGES<br>32 |
| 14. MONITORING AGENCY NAME & ADDRESS(if different from Controlling Office) | | 15. SECURITY CLASS. (of this report)<br>Unclassified<br>15a. DECLASSIFICATION/DOWNGRADING SCHEDULE |

16. DISTRIBUTION STATEMENT (of this Report)

Approved for public release; distribution unlimited.

17. DISTRIBUTION STATEMENT (of the abstract entered in Block 20, if different from Report)

18. SUPPLEMENTARY NOTES

19. KEY WORDS (Continue on reverse side if necessary and identify by block number)

Samara
Flexible fin
Autogyro
Decelerator
Maple seed

20. ABSTRACT (Continue on reverse side if necessary and identify by block number)

This report describes a simple decelerator which drives a submunition in a lunar motion while it descends vertically over a battlefield, scanning for armored targets. The decelerator, which consists of a single flexible fin with a weighted tip, evolved from the Improved Sensing Munitions (ISM) Exploratory Development Program conducted at U.S. Army Armament Research and Development Center.

(cont)

DD FORM 1 JAN 73 1473 EDITION OF 1 NOV 65 IS OBSOLETE

UNCLASSIFIED

SECURITY CLASSIFICATION OF THIS PAGE (When Data Entered)

20. ABSTRACT (cont)

The idea of using a flexible fin with a tip weight to generate a lunar scan motion was derived from the flight of maple seeds or samaras. Aerodynamic testing consisted of flying various configurations of the submunition in a vertical wind tunnel during which a nondimensional spin-to-velocity ratio of 0.110 and a drag coefficient of 3.21 (based on the submunition's diameter) were obtained. A simulation of the observed lunar motion of an axisymmetric model using a rolling body frame, six-degree-of-freedom (6-DOF) computer program, and estimates of the aerodynamic coefficients that could not be measured are presented.

CONTENTS

## FIGURES

## INTRODUCTION

A samara-type decelerator was developed by the U.S. Army Armament Research and Development Center to orient and stabilize scanning submunitions ejected from a spinning projectile in mid-to-late flight. The idea of using a single flexible fin with a tip weight to generate a lunar scan motion was derived from the flight of maple seeds or "samaras." The submunitions descend vertically over the battlefield, searching for armored targets. A spiral ground-scan footprint pattern is generated by the rotation of the cylindrical submunition about an axis tilted with respect to its axis of symmetry (fig. 1). When a target is detected, the firing train is initiated, and a penetrator is explosively formed and fired from the front face of the submunition.

The samara decelerator consists of a single flexible fin, with a tip weight typically between 2% and 5% of the body weight. It is attached to the top edge of the cylindrical submunition. The fin is mounted and shaped to give the camber, twist, and dihedral required for steady spin, descent velocity, and stability. Dispersion may be obtained by sequential deployment of the fin on each submunition. The packing volume is about 1/10th that of a deceleration system using a rotating parachute.

The effectiveness of the design was first demonstrated in free-flight testing of a small scale model, using a single flexible fin, in the vertical wind tunnel (VWT) at Wright Patterson Air Force Base, Ohio. Later testing with a full (dimensional) scale model in the VWT demonstrated a constant spin rate, descent velocity, and a scan angle near the design value of 30 degrees.

This report presents the results of VWT testing of the samara-body combination. A set of aerodynamic coefficients was estimated, then refined using a six-degree-of-freedom (6-DOF) computer program to simulate the motion observed in the VWT.

## DISCUSSION

### Submunition Physical Characteristics

The wind tunnel model (fig. 2) consisted of an approximately full (dimensional) scale, right circular cylinder made of Lexan (35% of the weight of an actual submunition) and a single flexible fin as an orientation and stabilization (O&S) device. The cylinder was 4.75-in. in diameter and 3.40-in. long. The flexible fin, made of a double layer of 3 oz/yd$^2$ nylon, had a 7.5-in. span and a 3-in. chord. It was attached at the edge of the cylindrical submunition body and weighted at the tip with a steel cylinder whose center of gravity (c.g.) was slightly forward of the mid-chord. (Subsequent testing showed the fin to be more stable, particularly during the spin-up phase, if the c.g. of the tip weight were located at the quarter-chord position. The model weighed 2.78 lb and the tip, 0.085 lb.

The physical characteristics of the wind tunnel model were evaluated with a computer program capable of calculating moments and products of inertia, center of gravity, mass, and the orientation of the principal axes of inertia for asymmetric bodies. For purposes of modeling, the submunition was treated as a rigid body with three parts: the cylindrical body, the flexible fin, and the tip weight. It was assumed that in flight, the orientation of the fin was normal to the spin axis, and the axis of symmetry of the body was tilted at the scan angle ($\alpha_{scan}$) to the spin axis (fig. 3). Computations were performed for different values of $\alpha_{scan}$ until the spin axis was aligned with a principal axis of inertia which is the axis about which the body would rotate in the absence of any external moments. The angle for this configuration was 31 degrees.

A set of curves was computed to show the effect of tip weight mass and fin length on the scan angle for a Lexan body (fig. 4) and an aluminum body (fig. 5). Increasing the tip weight and/or the fin length increases the scan angle, although the plots indicate a maximum angle of about 50 degrees for this size body.

**Wind Tunnel Testing**

The testing was conducted in the vertical wind tunnel (VWT) at the Air Force Wright Aeronautical Laboratory (AFWAL), Wright Patterson Air Force Base, Ohio. The VWT has a 12-foot open jet test section with an annular return and is capable of velocities up to 140 ft/s. The model was hand-launched with an initial spin rate to deploy the fin. Motion pictures were taken during test flights at 100 frames per second. The submunition in free flight is shown in figure 6. It flew at steady state conditions with a constant axial velocity of 77.0 ft/s and constant angular velocity of 47.1 rad/s. These values were determined from the motion pictures.

The drag coefficient ($C_D$) of 3.21 was based on body diameter. Model spin-up as a function of time was obtained from the VWT motion pictures (fig. 7). The curve starts at a nonzero spin rate because the models were prespun. The roll moment coefficients $C_\ell$ and the roll damping moment coefficients $C_{\ell_p}$ were obtained from a computer program which numerically solves the equation:

$$\dot{p} = \frac{\frac{1}{2}\rho V^2 Sd}{I_{xx}} \left[C_\ell + \left(C_{\ell_p}\right) \frac{pd}{2V}\right] \qquad (1)$$

The resulting $C_\ell$ was 0.282 and the $C_{\ell_p}$ varied between -1.59 and -2.45

After an initial transient period, the cylindrical body flew in a lunar motion at a constant angle-of-attack or scan angle of 25 degrees. The fin was oriented 10 degrees above the horizontal and was curved along the span. The steady state orientation of the submunition is shown in figure 8. The physical characteristics of the submunition with the fin in this orientation (about 35 degrees above the top of the body) were evaluated and the principal axes were

found to be rotated by 32 degrees with respect to the body axis of symmetry. The moments of inertia were:

| Body axes | Principal axes |
|---|---|
| $I_{xx}$ = 13.65 lb-in.$^2$ | $I_{xp}$ = 16.51 lb-in.$^2$ |
| $I_{yy}$ = 9.36 lb-in.$^2$ | $I_{yp}$ = 6.64 lb-in.$^2$ |
| $I_{zz}$ = 15.49 lb-in.$^2$ | $I_{zp}$ = 15.49 lb-in.$^2$ |
| $I_{xy}$ = -4.39 lb-in.$^2$ | |

As previously stated, the body was rotating about an axis other than the principal axis. Euler's equations of motion for a rigid body rotating about a fixed point state that a body will rotate about a principal axis of inertia unless an external moment is acting on the body. This moment is given by:

$$M_z = I_{zp}\,\dot{\omega}_{zp} - I_{xp}\,\omega_{xp}\,\omega_{yp} + I_{yp}\,\omega_{yp}\,\omega_{xp}$$

At steady state, $\dot{\omega}_{zp} = 0$; therefore

$$M_z = (I_{yp} - X_{xp})\,\omega_{xp}\,\omega_{yp}$$

Substituting for the principal inertias and angular velocity components, the external moment was 6.78 in.-lb. This moment is caused by the fin drag acting at the fin-body junction.

**Computer Simulation**

The flight of the submunition was modeled by use of a 6-DOF computer simulation (ref 1). This program is capable of using a body-fixed or fixed plane coordinate system and can handle aerodynamic and geometric asymmetries. To simulate the motion observed in the VWT, a body-fixed coordinate system was used. The orientation of the body axes with respect to the fixed inertial (Earth) coordinates is described by three Euler angles ($\psi$ the first rotation, $\theta$ the second, and $\phi$ the third). The body axes (shown aligned with the inertial earth axes); the positive sense of pitch, yaw, and spin rates, and the Euler angles are shown in figure 9.

The basic aerodynamic coefficients used in the program are defined in an aeroballistic system for symmetric missiles. However, the presence of the flexible fin on the body makes it highly nonsymmetric. Fortunately, the program also includes terms for aerodynamic asymmetries: the moment coefficients $C_{m_o}$ and $C_{n_o}$ and the force coefficients $C_{Y_o}$ and $C_{Z_o}$. The positive sense of the aerodynamic forces and moments are shown in figure 10. The angular equations of motion used in the program are

$$I_{xx}\,\dot{p} = I_{xy}(\dot{q} - pr) - (I_{zz} - I_{yy})qr + M_x \tag{2}$$

$$I_{yy}\,\dot{q} = I_{xy}(\dot{p} + qr) - (I_{xx} - I_{zz})pr + M_y \tag{3}$$

$$I_{zz}\,\dot{r} = I_{xy}(p^2 - q^2) + (I_{xx} - I_{yy})pq + M_z \tag{4}$$

where the aerodynamic moments are

$$M_x = \frac{1}{2}\rho V^2\, Sd\, \left[C_\ell + C_{\ell_p}\left(\frac{pd}{2V}\right)\right] \tag{5}$$

$$\begin{aligned} M_y = \frac{1}{2}\rho V^2\, Sd\, \{ & C_m \sin\xi + C_{m_p}\left(\frac{pd}{2V}\right)\cos\xi \\ & + C_{m_q}\left[\left(\frac{qd}{2V}\right)\sin^2\xi - \left(\frac{rd}{2V}\right)\cos\xi\sin\xi\right] \\ & + C_{n_r}\left[\left(\frac{qd}{2V}\right)\cos^2\xi + \left(\frac{rd}{2V}\right)\sin\xi\cos\xi\right] \\ & + C_{m_o}\} \end{aligned} \tag{6}$$

$$\begin{aligned} M_z = \frac{1}{2}\rho V^2\, Sd\, \{ & -C_m\cos\xi + C_{m_p}\left(\frac{pd}{2V}\right)\sin\xi \\ & - C_{m_q}\left[\left(\frac{qd}{2V}\right)\sin\xi\cos\xi - \left(\frac{rd}{2V}\right)\cos^2\xi\right] \\ & + C_{n_r}\left[\left(\frac{qd}{2V}\right)\cos\xi\sin\xi + \left(\frac{rd}{2V}\right)\sin^2\xi\right] \\ & + C_{n_o}\} \end{aligned} \tag{7}$$

As observed in the VWT test, the body flew at a constant scan angle (angle-of-attack) of 25 degrees and a constant angular velocity of 7.5 Hz. This motion, in terms of the Euler angles and angular rates, is

| | |
|---|---|
| $\psi$ = variable | $\dot{\psi}$ = 47.1 rad/s |
| $\theta$ = -65 degrees | $\dot{\theta}$ = 0 |
| $\phi$ = 90 degrees | $\dot{\phi}$ = 0 |

and

$$p = 42.7 \text{ rad/s} \qquad \dot{p} = 0$$

$$q = 19.9 \text{ rad/s} \qquad \dot{q} = 0$$

$$r = 0.0 \text{ rad/s} \qquad \dot{r} = 0$$

Noting that $\xi = 0$ at steady state and substituting equations 5, 6, and 7 into equations 2, 3, and 4,

$$C_{\ell} + C_{\ell_p} \frac{pd}{2V} = 0 \tag{8}$$

$$C_{m_p} \frac{pd}{2V} + C_{n_r} \frac{qd}{2V} + C_{m_o} = 0 \tag{9}$$

$$\frac{1}{2} \rho V^2 \, Sd \, (C_{n_o} - C_m) = (I_{yy} - I_{xx}) \, pq + I_{xy} \, (p^2 - q^2) \tag{10}$$

Substituting the numerical values of p, q, $I_{xx}$, etc. into 8, 9 and 10, the following steady state relationships result:

$$C_{\ell} + 0.11 \, C_{\ell_p} = 0 \tag{11}$$

$$0.11 \, C_{m_p} + 0.051 \, C_{n_r} + C_{m_o} = 0 \tag{12}$$

$$C_{n_o} - C_m = 1.65 \tag{13}$$

From the wind tunnel test, $C_{\ell}$ was estimated to be 0.282 and solving equation 11 at steady state, $C_{\ell_p} = -2.57$. The drag coefficient at steady state was 3.21, but there was no way of obtaining the lift coefficient from the wind tunnel test. For purposes of this simulation, it was assumed that the lift coefficient was zero and the drag coefficient did not depend on the angle-of-attack ($\alpha$) so that

$$C_X = C_D \cos \alpha \tag{14}$$

$$C_N = C_D \sin \alpha \tag{15}$$

Pitching moment coefficients ($C_m$) for the cylindrical body alone were obtained from references 2 and 3. At $\alpha = 25$ degrees, $C_m = -0.087$ and solving equation 13, $C_{n_o} = 1.559$ at steady state. It is assumed that $C_{n_o}$ does not depend on $\alpha$ since it appears that only the body changes angle-of-attack in flight while the flexible fin is always oriented perpendicular to the spin axis and, therefore, generates a constant moment. The remaining coefficients ($C_{m_p}$, $C_{m_o}$, $C_{n_r}$, $C_{m_q}$) were obtained in an iterative manner: The damping moment coefficients $C_{n_r}$ and $C_{m_q}$ were chosen and made equal; a value was chosen for $C_{m_o}$, and equation 12 was solved for the Magnus moment coefficient ($C_{m_p}$); $C_{m_o}$ was assumed constant, and $C_{m_p}$ assumed linear with $\alpha$. The program was run using the initial conditions from the wind tunnel test: initial velocity of 77 ft/s, initial spin rate of 25.1 rad/s, and an angle-of-attack of 0 degrees. This process was repeated until the transient motion damped out in 2 or 3 seconds and the computed motion agreed with the observed motion. A summary of a successful set of coefficients (based on the cross sectional body area) is shown in table 1. A plot of scan angle versus time for a simulation run with these coefficients is shown in figure 11. Note that other combinations of coefficients ($C_{m_p}$, $C_{m_o}$, $C_{n_r}$, $C_{m_q}$) would have produced an acceptable match of the wind tunnel results.

## CONCLUSIONS

1. A simple orientation and stabilization device for a slow, steady scanning flight has been described. The device consists of a single flexible fin and a tip weight which is used to drive the submunition in a lunar motion.

2. The scan angle was found to increase with the length of the fin and/or the mass of the tip weight.

3. A set of aerodynamic coefficients has been determined for the submunition which was adequate to simulate the motion observed in the wind tunnel on a six-degree-of-freedom computer program. More testing is required to verify those coefficients and to determine the effect of angle-of-attack and Mach number variations on the coefficients.

Table 1. Six-degree-of-freedom aerodynamic coefficients

| | Angle of attack (degrees) | | | | | | | | | |
|---|---|---|---|---|---|---|---|---|---|---|
| | 0 | 10 | 20 | 30 | 40 | 50 | 60 | 70 | 80 | 90 |
| $C_x$ | -3.21 | -3.17 | -3.02 | -2.78 | -2.46 | -2.07 | -1.61 | -1.10 | -0.56 | 0.0 |
| $C_N$ | 0.0 | 0.56 | 1.10 | 1.61 | 2.07 | 2.46 | 2.78 | 3.02 | 3.17 | 3.21 |
| $C_m$ | 0.0 | -0.037 | -0.063 | -0.067 | -0.051 | -0.044 | -0.042 | -0.023 | -0.016 | 0.0 |
| $C_{m_q}$ | -10.0 | ---------- | | | | | | | | -10.0 |
| $C_{m_p}$ | 0.0 | 2.22 | 4.44 | 6.66 | 8.88 | 11.10 | 13.32 | 15.54 | 17.76 | 19.98 |
| $C_\ell$ | 0.28 | ---------- | | | | | | | | 0.28 |
| $C_{\ell_p}$ | -2.57 | ---------- | | | | | | | | -2.57 |
| $C_{m_o}$ | -0.10 | ---------- | | | | | | | | -0.10 |
| $C_{n_o}$ | 1.56 | ---------- | | | | | | | | 1.56 |

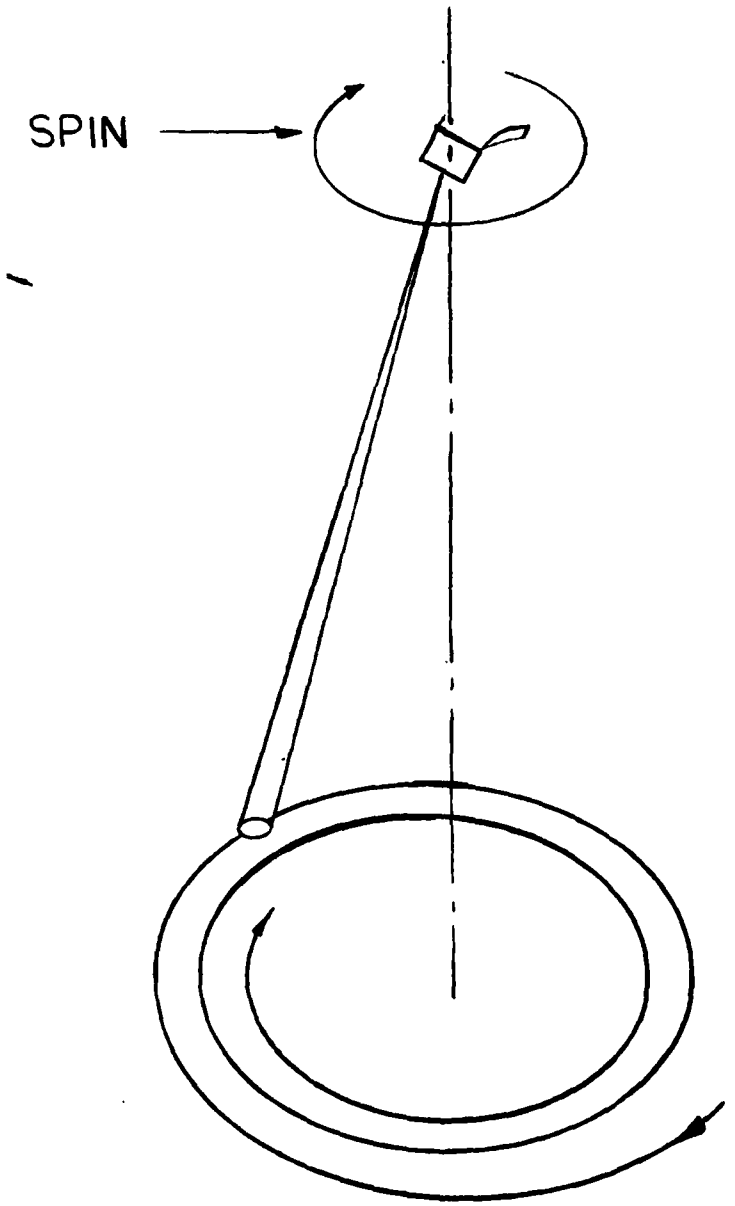


Figure 1. Submunition, descending and scanning

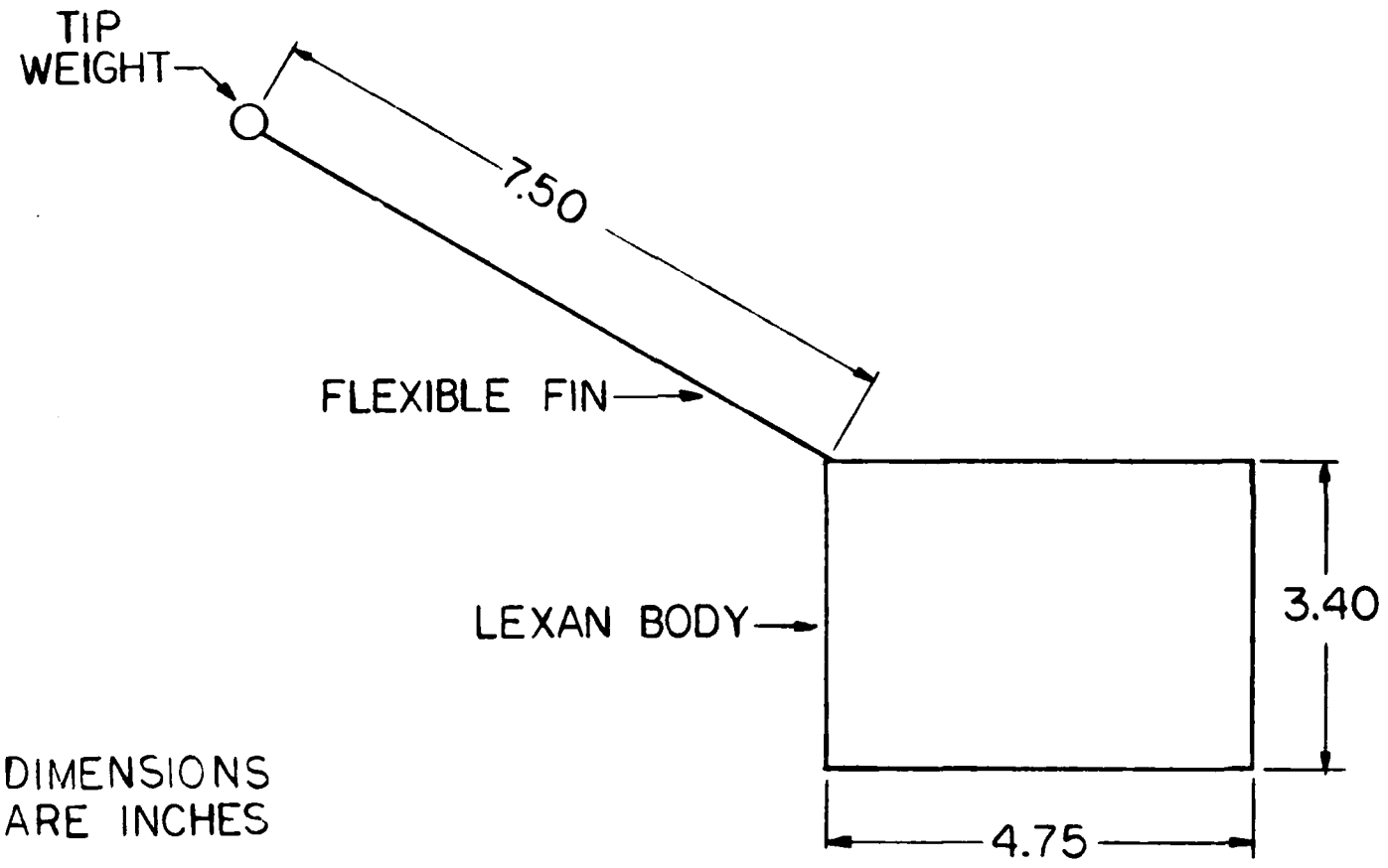


Figure 2. Wind tunnel model

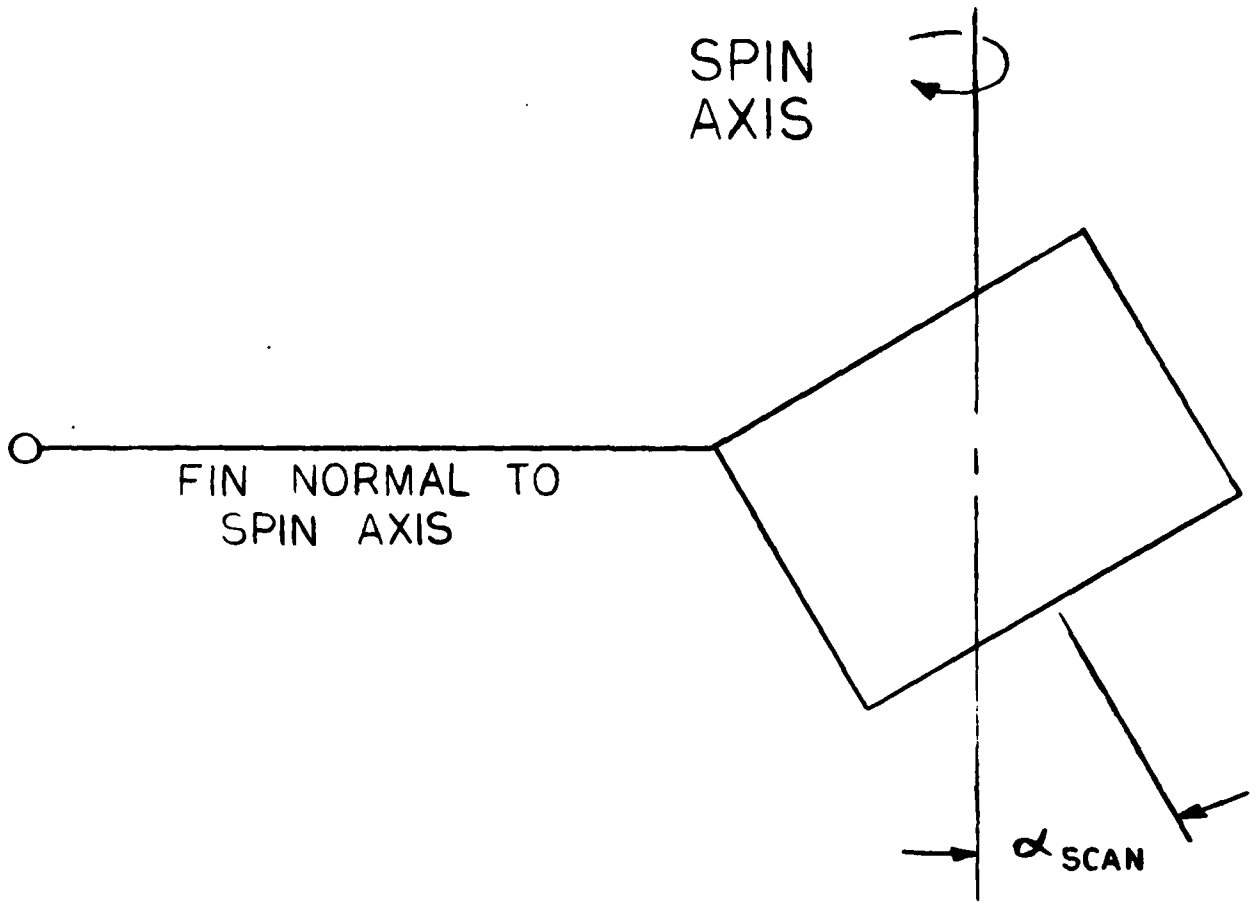


Figure 3. Assumed orientation of the submunition for the mass properties program

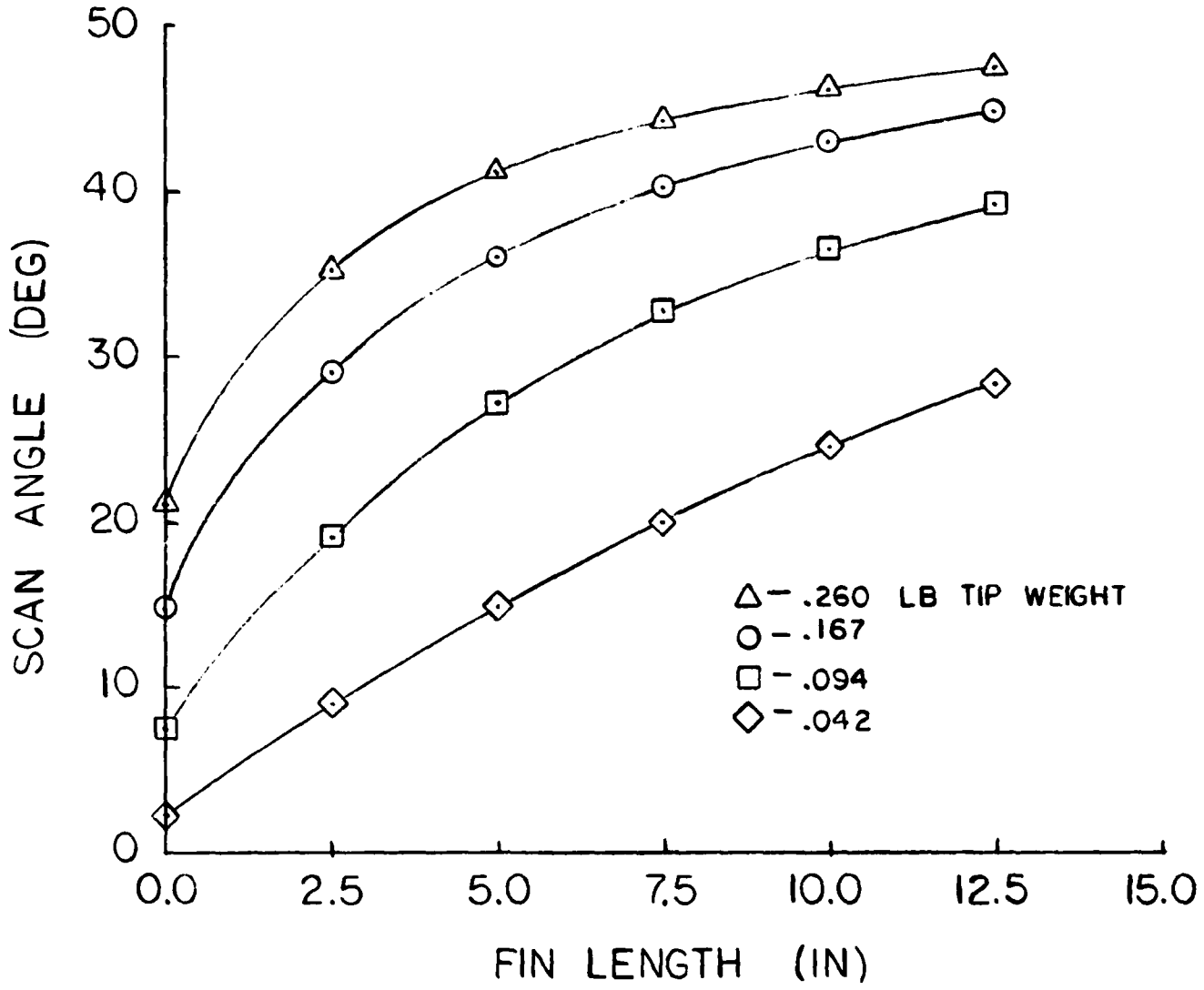


Figure 4. The effect of fin length and tip weight on the submunition scan angle for a Lexan body

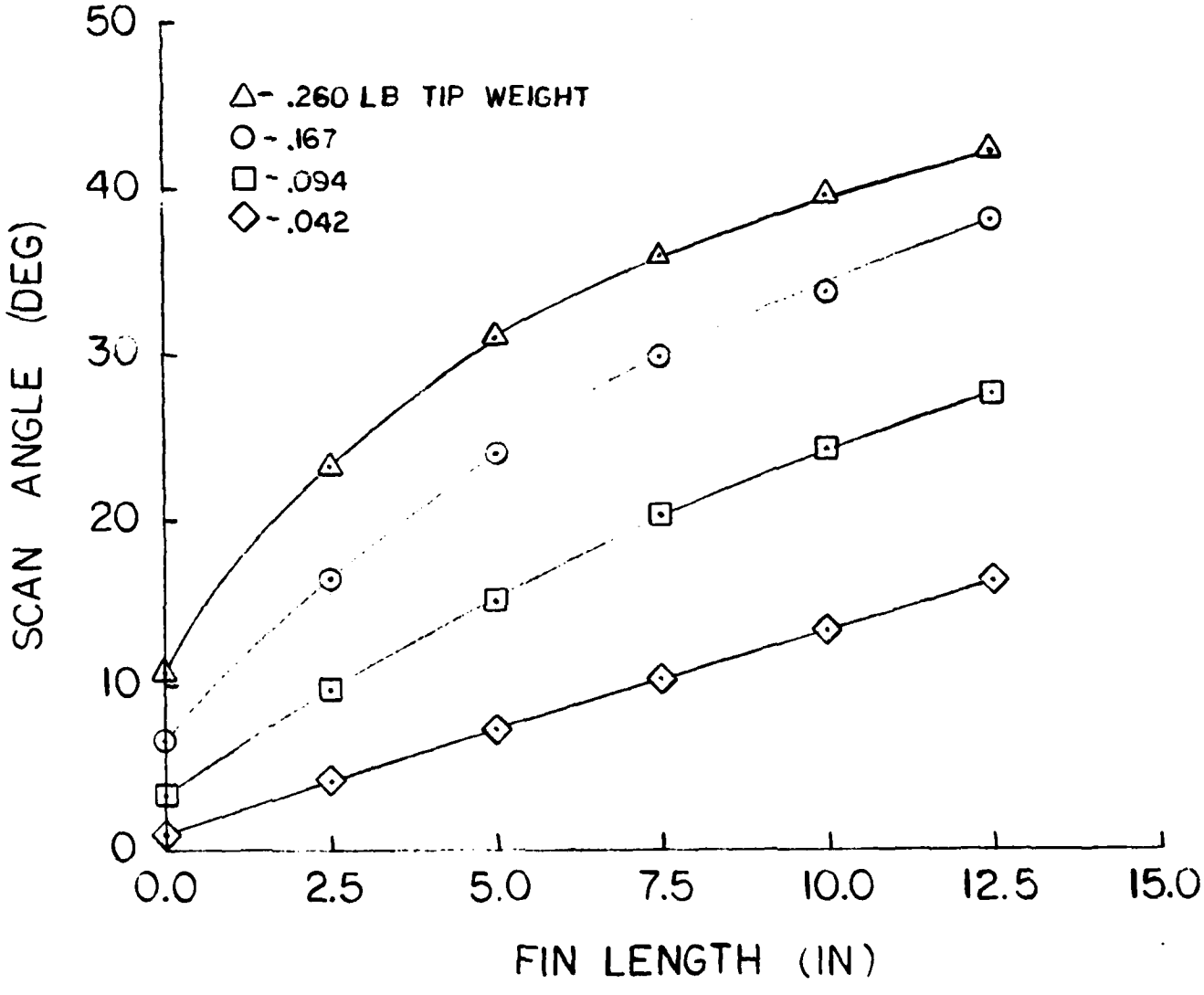


Figure 5. The effect of fin length and tip weight on the submunition scan angle for an aluminum body

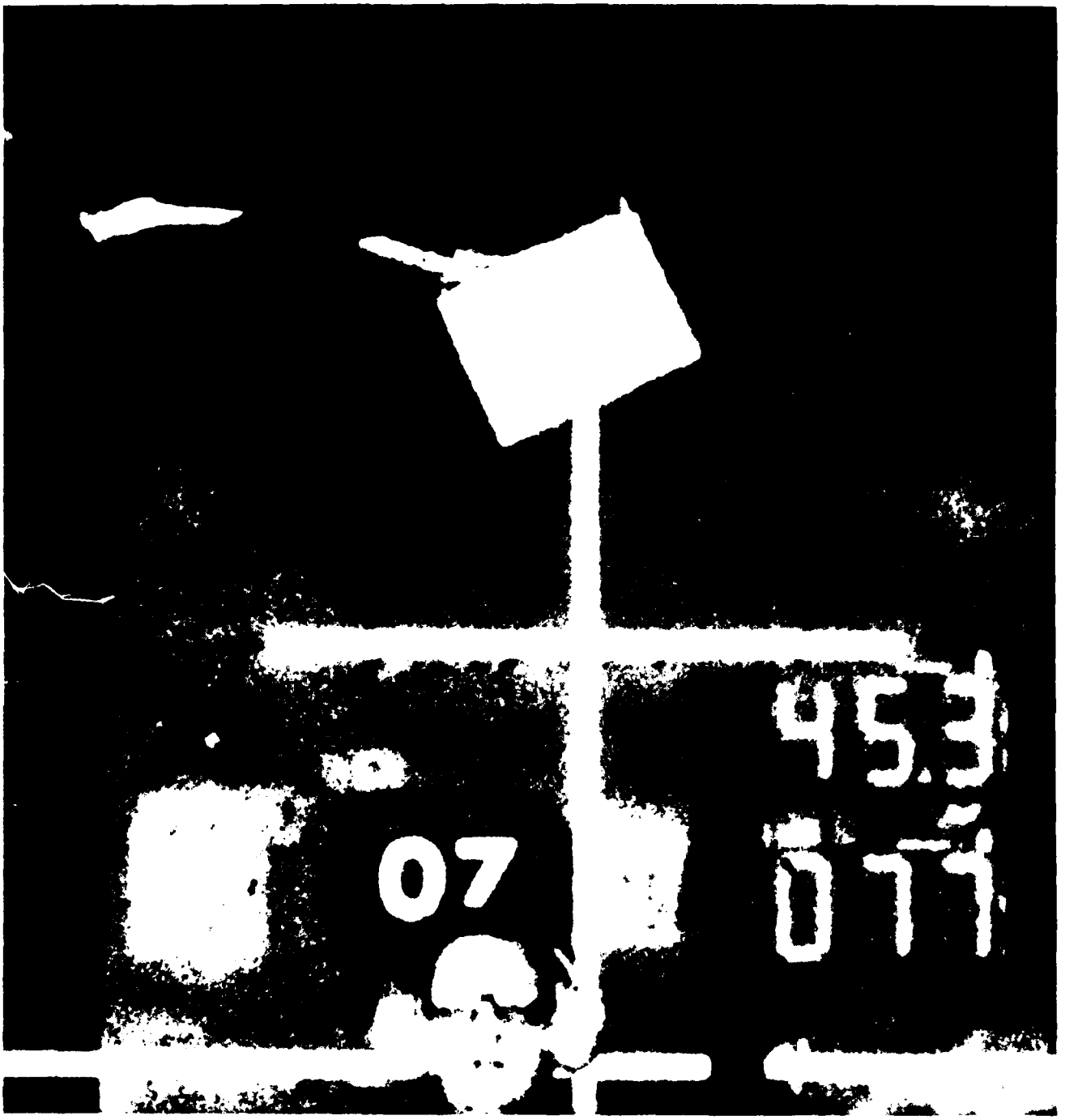


Figure 6. The wind tunnel model in free flight in the vertical wind tunnel

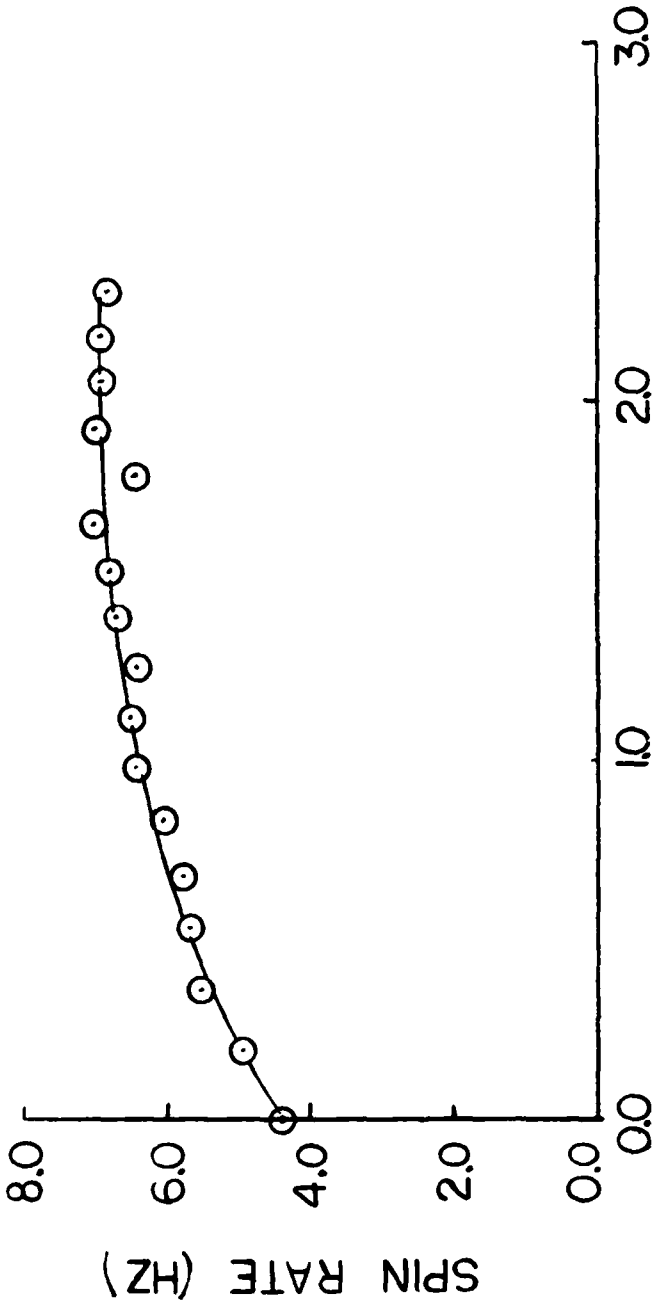


Figure 7. Wind tunnel model spin-up as a function of time

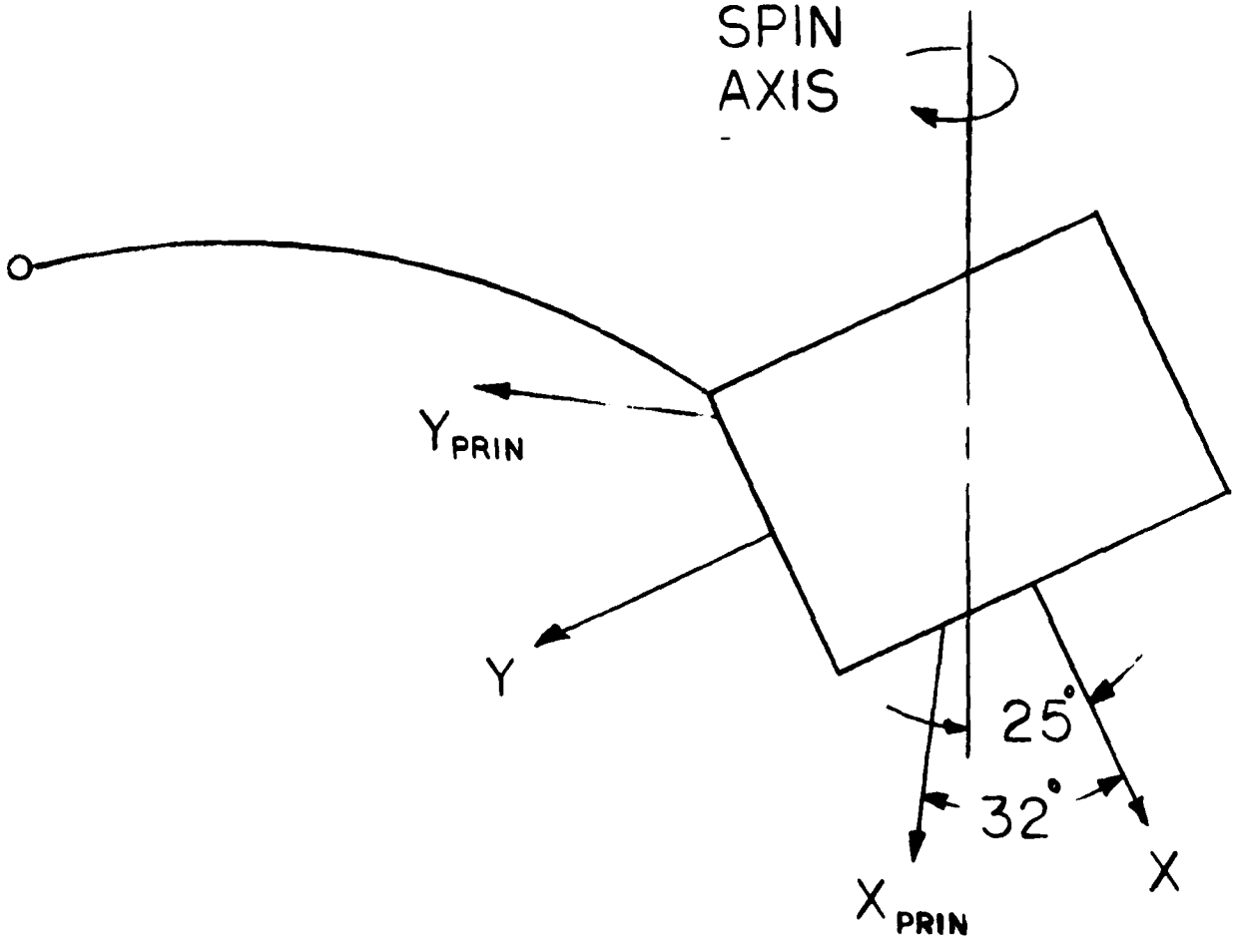


Figure 8. The steady-state orientation of the wind tunnel model

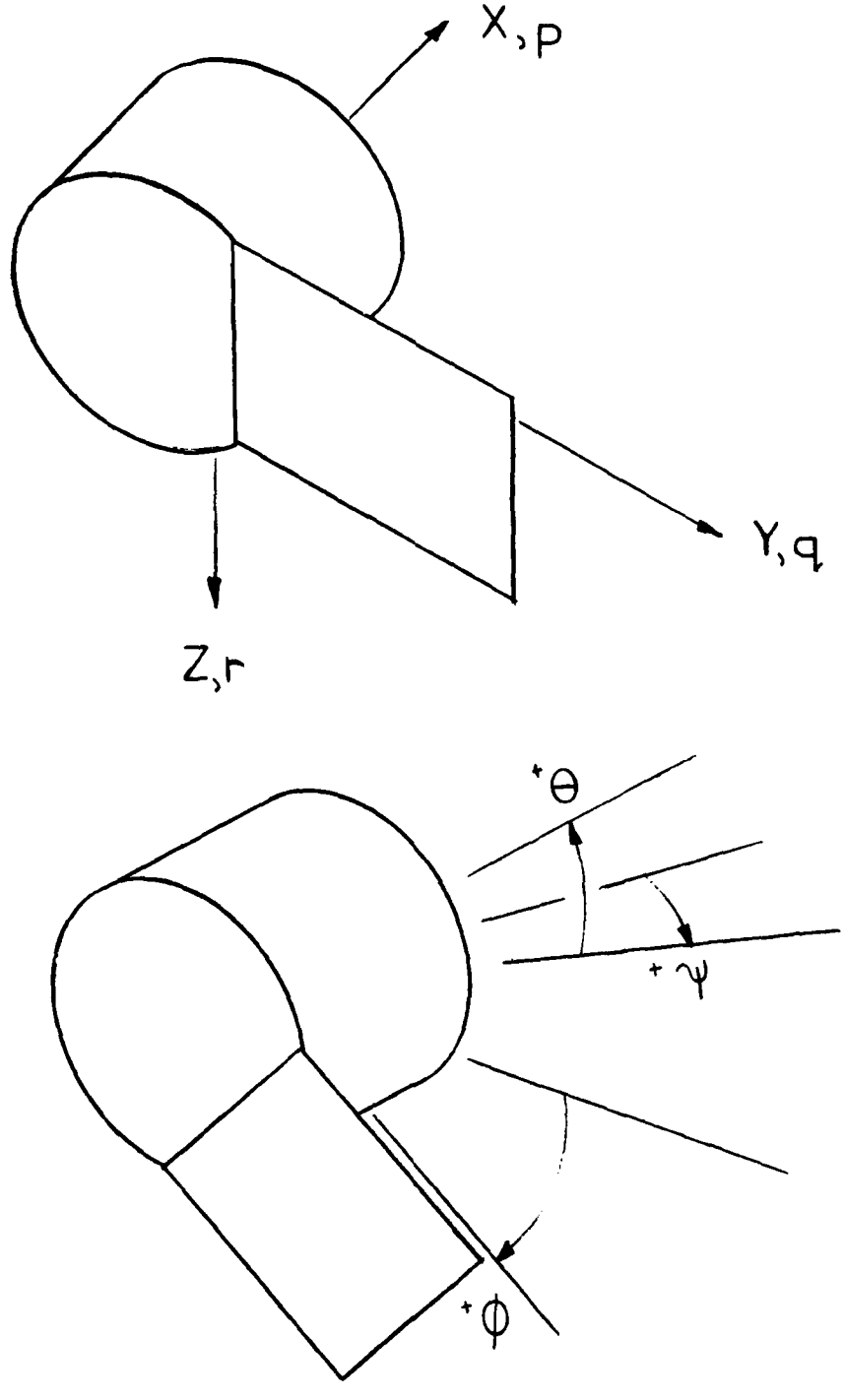


Figure 9. Sign conventions and Euler angles used in the six-degree-of-freedom simulation

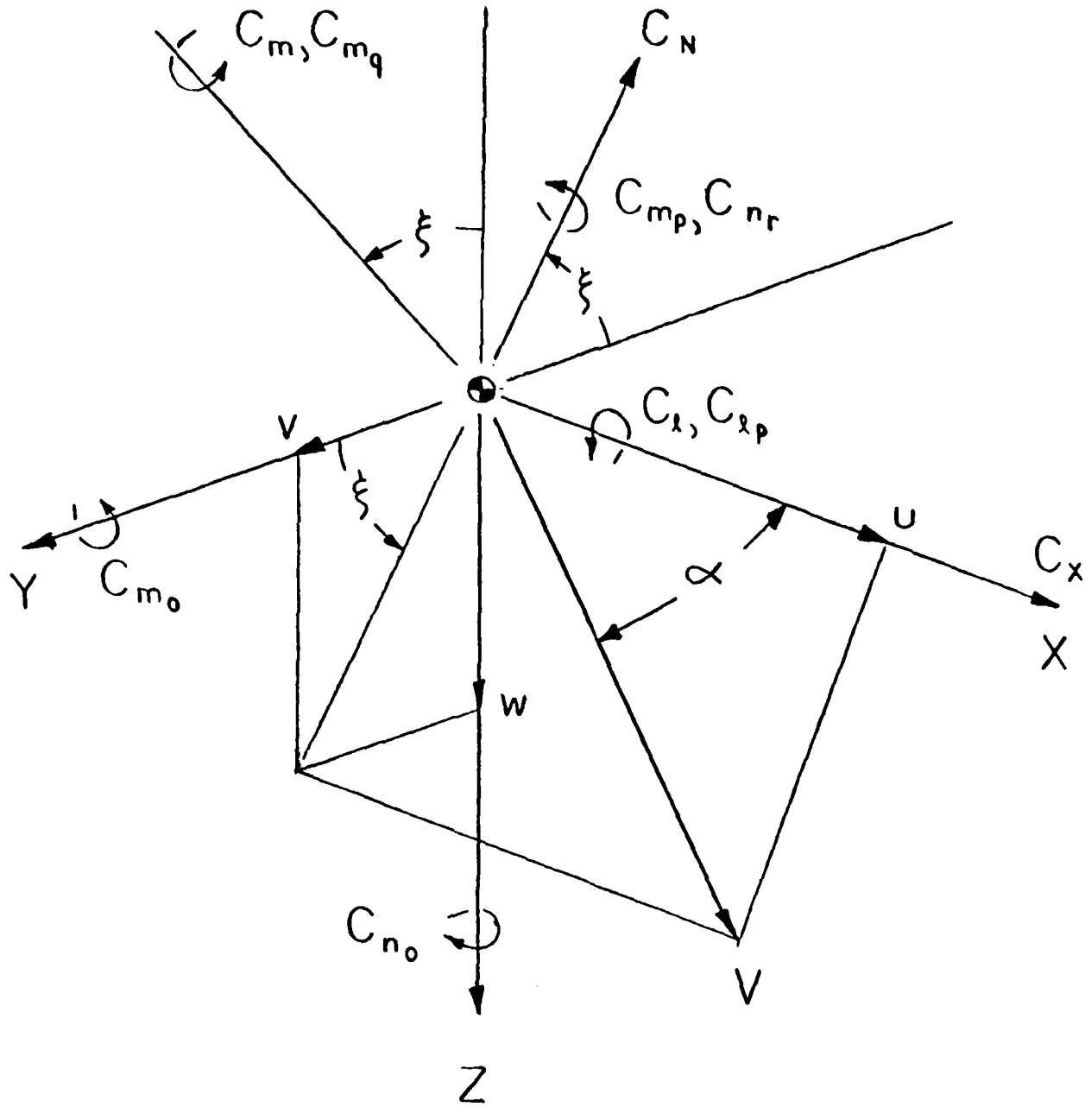


Figure 10. Aerodynamic forces and moments used in the six-degree-of-freedom simulation

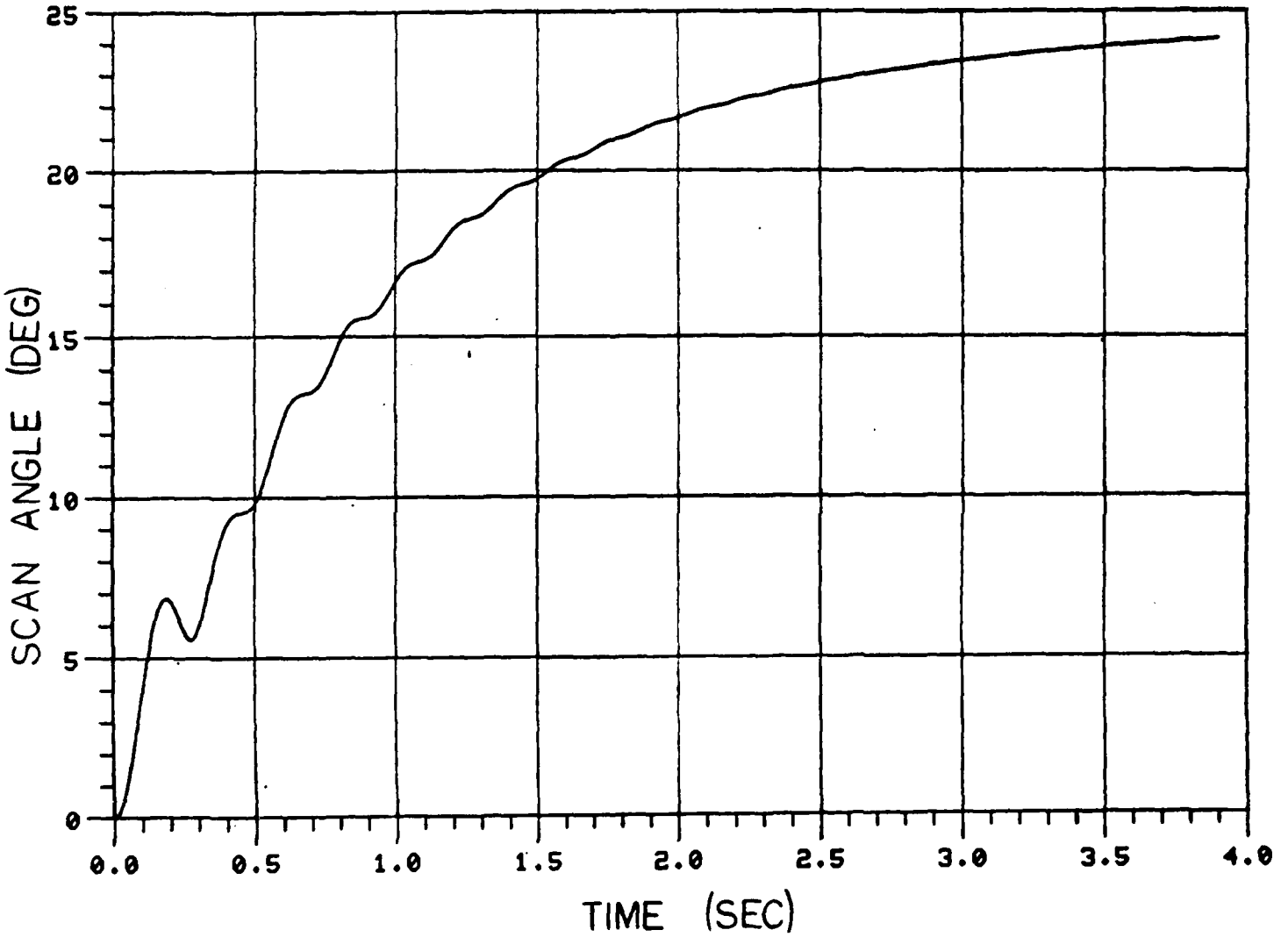


Figure 11. Six-degree-of-freedom computer simulation of submunition angle-of-attack given the initial conditions of the vertical wind tunnel test

## REFERENCES


1. J. E. Brunk, "6-DOF Monte Carlo Trajectory Program," Report No. 72-0089-10, Alpha Research, Inc., Santa Barbara, CA, September 1972.

2. W. C. Hayes, Jr. and W. P. Henderson, "Some Effects of Nose Bluntness and Fineness Ratio on the Static Longitudinal Aerodynamic Characteristics of Bodies of Revolution at Subsonic Speeds," NASA TN D-650, February 1961.

3. R. W. Rhudy and S. S. Baker, "Static Stability and Axial-Force Characteristics of Several Flat-Faced Right Circular Cylinders at Subsonic and Supersonic Speeds and Angles of Attack From 0 to 90 Degrees," AEDC-TR-72-180, January 1973.

## SYMBOLS

$C_D$ Drag coefficient, $\frac{D}{QS}$

$C_\ell$ Roll moment coefficient, $\frac{L}{QSd}$

$C_{\ell_p}$ Roll damping moment coefficient derivative, $\frac{1}{QSd}\left[\frac{\Delta L_p}{\Delta \frac{pd}{2v}}\right]$

$C_m$ Pitching moment coefficient (angle-of-attack plane), $\frac{M}{QSd}$

$C_{m_p}$ Magnus moment coefficient derivative, $\frac{1}{QSd}\left[\frac{\Delta M_p}{\Delta \frac{pd}{2v}}\right]$

$C_{m_q}$ Damping moment coefficient derivative (angle-of-attack plane), $\frac{1}{QSd}\left[\frac{\Delta M_q}{\Delta \frac{qd}{2v}}\right]$

$C_{m_o}$ Trim moment coefficient about Y-body axis, $\frac{M_o}{QSd}$

$C_N$ Normal force coefficient, $\frac{N}{QS}$

$C_{n_r}$ Damping moment coefficient derivative (Magnus plane), $\frac{1}{QSd}\left[\frac{\Delta n_r}{\Delta \frac{rd}{2v}}\right]$

$C_{n_o}$ Trim moment coefficient about Z-body axis, $\frac{n_o}{QSd}$

$C_X$ Axial force coefficient, $\frac{X}{QS}$

$C_{Y_o}$ Trim force coefficient along Y-body axis, $\frac{Y_o}{QS}$

$C_{Z_o}$ Trim force coefficient along Z-body axis, $\frac{Z_o}{QS}$

c.g. Center of gravity

d Reference diameter, equal to submunition diameter

D Drag force

$I_{xx}$ Moment of inertia about x body axis, through the c.g.

$I_{xp}$ Moment of inertia about x principal axis

$I_{xy}$ Product of inertia in the x-y plane

$I_{yp}$ Moment of inertia about y principal axis

$I_{yy}$ Moment of inertia about y body axis, through the c.g.

$I_{zp}$ Moment of inertia about z principal axis

$I_{zz}$ Moment of inertia about z body axis, through c.g.

L Rolling moment

$L_p$ Roll damping moment

M Pitching moment

$M_p$ Magnus moment

$M_q$ Damping moment, angle-of-attack plane

$M_o$ Trim moment

N Normal force

$n_r$ Damping moment, magnus plane

$n_o$ Trim moment

$M_x$ Total moment about x body axis

$M_y$ Total moment about y body axis

$M_z$ Total moment about z body axis

p Spin rate

$\dot{p}$ Time rate of change of spin rate

q Pitch rate

$\dot{q}$ Time rate-of-change of pitch rate

Q Dynamic pressure, $\frac{1}{2} \rho v^2$

r Yaw rate

$\dot{r}$ Time rate-of-change of yaw rate

S Reference area, $\pi \frac{d^2}{4}$

u Component of velocity in X-body direction

V Total velocity

v Component of velocity in Y-body direction

w Component of velocity in Z-body direction

X Body coordinate

Y Body coordinate

$Y_o$ Trim force

Z Body coordinate

$Z_o$ Trim force

$\alpha$ Angle-of-attack

$\alpha_{scan}$ Scan angle

$\theta$ Second Euler rotation

$\xi$ Orientation of cross velocity, $\cos \xi = \frac{v}{\sqrt{v^2 + w^2}}$

$\rho$ Atmospheric density

$\phi$ Third Euler rotation

$\psi$ First Euler rotation

$\omega_{xp}$ Component of angular velocity along x principal axis of composite body

$\omega_{yp}$ Component of angular velocity along y principal axis of composite body

$\omega_{zp}$ Component of angular velocity along z principal axis of composite body

## DISTRIBUTION LIST

Commander
Armament Research and Development Center
U.S. Army Armament, Munitions
and Chemical Command
ATTN: SMCAR-AE, B. W. Bushey
SMCAR-AET, W. Ebihara (2)
SMCAR-AET-A, A. Loeb
D. Mertz (2)
R. Kline
W. Koenig (10)
SMCAR-FFP, E. Zimpo
SMCAR-FFP-I, R. Reisman
V. Marchese
SMCAR-MSI (5)
Dover, NJ 07801-5001

Commander
U.S. Army Armament, Munitions
and Chemical Command
ATTN: AMSMC-GCL(D)
Dover, NJ 07801-5001

Administrator
Defense Technical Information Center
ATTN: Accessions Division (12)
Cameron Station
Alexandria, VA 22304-6145

Director
U.S. Army Materiel Systems
Analysis Activity
ATTN: AMXSY-MP
Aberdeen Proving Ground, MD 21005-5066

Commander
Chemical Research and Development Center
U.S. Army Armament, Munitions
and Chemical Command
ATTN: SMCCR-SPS-IL
Aberdeen Proving Ground, MD 21010-5423

Commander
Chemical Research and Development Center
U.S. Army Armament, Munitions
and Chemical Command
ATTN: SMCCR-RSP-A
Aberdeen Proving Ground, MD 21010-5423

Director
Ballistic Research Laboratory
ATTN: AMXBR-OD-ST
AMXBR-LFD, C. Murphy
L. MacAllister
W. Mermegan
V. Oskay
Aberdeen Proving Ground, MD 21005-5066

Chief
Benet Weapons Laboratory, CCAC
Armament Research and Development Center
U.S. Army Armament, Munitions
and Chemical Command
ATTN: SMCAR-CCB-TL
Watervliet, NY 12189-5000

Commander
U.S. Army Armament, Munitions
and Chemical Command
ATTN: AMSMC-ESP-L
Rock Island, IL 61299-6000

Director
U.S. Army TRADOC Systems
Analysis Activity
ATTN: ATAA-SL
White Sands Missile Range, NM 88002

Commander
Harry Diamond Laboratories
ATTN: DELHD-TI, Library
2800 Powder Mill Road
Adelphi, MD 20783-1197

Director
Advanced Research Projects Agency
Department of Defense
Washington, DC 20301

Chief
Bureau of Naval Weapons
Department of the Navy
ATTN: DIS-33
Washington, DC 20360

Commander
Naval Ordnance Systems Command
ATTN: ORD 0323B1, J. V. Costello
Washington, DC 20360

Commandant
Marine Corps Development Center
ATTN: Firepower Division
Quantico, VA 22134

Commander
Marine Corps
Department of the Navy
ATTN: A04F
Washington, DC 20360

Commander
U.S. Naval Surface Weapons Center
White Oak Laboratory
ATTN: Research Library
White Oak, Silver Spring, MD 20910

Commander
U.S. Naval Ship Research
and Development Center
ATTN: Aerodynamics Laboratory
Washington, DC 20007

Department of the Army
Office, Chief of Research Development
and Acquisition
ATTN: DAMA-CSS-N
DAMO-SSN
Washington, DC 20310

Commander
U.S. Army Materiel Command
ATTN: AMCDRD-RS-PE-BAL
5001 Eisenhower Avenue
Alexandria, VA 22304

Commander
U.S. Army Missile Command
U.S. Army Missile Laboratory
ATTN: AMSMI-RDK
Redstone Arsenal, AL 35898-5252

Commander
U.S. Naval Weapons Center
ATTN: Code 5557
Technical Library
China Lake, CA 93555

Commander
Air Proving Ground Center (PGTRI)
ATTN: Technical Library
Eglin Air Force Base, FL 32542

Commander
U.S. Naval Surface Weapons Center
Dahlgren Laboratory
ATTN: Technical Library
Dahlgren, VA 22448

Director
NASA Ames Research Center
ATTN: Technical Library
Moffett Field, CA 94035

Director
U.S. Army Aeronautical Laboratory
Moffett Field, CA 94035

Headquarters
Air Force Weapons Laboratory
ATTN: Technical Library
Kirtland Air Force Base, NM 87117

Avco Corporation
Avco Systems Division
ATTN: T. Kane
201 Lowell Street
Wilmington, MA 01887

Aerojet ElectroSystems
ATTN: D. Pillasch
1100 West Hollyvale Street
Asusa, CA 91702

Honeywell, Inc.
Defense Systems Division
ATTN: G. Stilley
10400 Yellow Circle Drive
Minnetonka, MN 55343